Spin Correlation Functions in $Cu(NH_3)_4PtCl_4$ †

Z. G. Soos* and T. Z. Huang
Department of Chemistry, Princeton University, Princeton, New Jersey 08540
J. S. Valentine
Department of Chemistry, Douglass College, Rutgers University, New Brunswick, New Jersey 08903
R. C. Hughes
Sandia Laboratories, Albuquerque, New Mexico 87115
(Received 12 March 1973)

The angular dependence of the exchange-narrowed Lorentzian EPR line in $Cu(NH_3)_4PtCl_4$, a crystal with magnetically equivalent square planar $Cu(NH_3)_4^{++}$ sites, is shown to provide a direct evaluation of several high-temperature Fourier components of the spin autocorrelation function $C(t) = 4\langle S_i^x(t)S_i^x(0)\rangle$ and of $C^2(t)$. The angular dependence of the "10/3" effect observed at X and Q bands supports the Blume-Hubbard model for spin correlation functions. The enhanced $\omega = 0$ Fourier components are consistent with largely one-dimensional exchange in $Cu(NH_3)_4PtCl_4$ and the $\omega = 0$ component of the four-spin correlations $\langle S_i^x(t)S_{i+1}^x(t)S_{i+1}^x(0)S_i^x(0)\rangle$ satisfies a numerical bound due to Carboni and Richards for finite one-dimensional chains. The method is applicable to any exchange-coupled paramagnetic crystals with magnetically equivalent sites and provides a direct test for theoretical models of spin correlation functions.

I. INTRODUCTION

Isotropic, or very nearly isotropic, exchange interactions occur in a wide variety of inorganic crystals[1] containing paramagnetic ions and in many organic free-radical solids.[2] An effective Heisenberg exchange Hamiltonian[3]

$$\mathcal{H}_e = \sum_{i<j} J_{ij}\vec{S}_i \cdot \vec{S}_j \tag{1}$$

describes the electrostatic interactions between weakly overlapping orbitally nondegenerate sites with spins $\vec{S}_i$. In most cases of interest, the exchange constants J_{ij} are significantly larger than spin-spin interactions such as dipolar or hyperfine couplings. The exchange then dominates the spin dynamics. Both neutron-diffraction[4] and magnetic-resonance[5] studies sample Fourier components of spin correlation functions and have focussed attention on the general questions of spin dynamics arising from $\mathcal{H}_e$. The normalized two-spin correlation function

$$C_{ij}(t) = [3/S(S+1)]\langle S_i^x(t)S_j^x(0)\rangle \tag{2}$$

has been investigated primarily for the case $i=j$, with $C(t) \equiv C_{ii}(t)$. The two-spin autocorrelation function $C(t)$ has been computed by Windsor[6] for classical spins, by Blume and Hubbard[7] at high temperature, and by Carboni and Richards[8] for finite linear chains. A Gaussian form for $C(t)$ was originally suggested by Anderson and Weiss[9] for exchange-coupled spins. The time evolution of $S_i^x(t)$ is given by $\mathcal{H}_e$,

$$S_i^x(t) = e^{i\mathcal{H}_e t/\hbar} S_i^x(0) e^{-i\mathcal{H}_e t/\hbar} \quad . \tag{3}$$

In Eq. (2), $\langle\rangle$ denotes the thermal average. The two-spin correlation function $C_{ij}(t)$ thus occurs in a variety of paramagnetic solids. Neutron diffraction involves the two-spin correlation functions and is consequently simpler to analyze than the exchange narrowing of EPR lines, where electron dipolar interactions require four-spin correlations. The analysis of EPR linewidths has nevertheless provided information about spin correlations, especially in the special case of one-dimensional exchange encountered in $(CH_3)_4NMnCl_3$ (TMMC)[10] and various copper salts.[11]

We show here that the angular dependence of the high-temperature EPR linewidth provides a simple direct method for obtaining Fourier components of spin correlation functions in exchange-coupled systems. The method is illustrated for $Cu(NH_3)_4PtCl_4$, hereafter called CTP. CTP provides several important advantages over previously studied copper salts, the most important of which is that the square-planar copper tetrammine (CT) complexes are magnetically equivalent.

The central idea of the present method is to take advantage of the isotropy of $\mathcal{H}_e$ in spin space, regardless of the form of the exchange constants $J_{ij} = J(\vec{r}_{ij})$. The spin correlation functions then satisfy[7]

$$\langle S_i^\alpha(t)S_j^\beta(0)\rangle = \delta_{\alpha\beta}\langle S_i^x(t)S_i^x(0)\rangle \tag{4}$$

for $\alpha, \beta = x, y, z$. The general theories of magnetic resonance[5,8] relate the width of an exchange-narrowed line to the amplitude of local (dipolar and hyperfine) fields and, for $kT \gg J_{ij}$, to Fourier components of spin correlation functions. The angular

dependence of the local-field amplitudes can readily be computed via the second moment and are summarized in Table I for CTP. Since the spin correlations arising from $\mathcal{H}_e$ are isotropic, the angular dependence of the EPR linewidth provides equations in which the only unknowns are Fourier components of various spin correlation functions. In Sec. IV we obtain Fourier components of $C(t)$ and of $C^2(t)$ which, for $\omega \neq 0$, are in agreement with either the Blume-Hubbard[7] or the Anderson-Weiss[9] function. The $\omega = 0$ components are not correctly predicted by these models and reflect the largely one-dimensional exchange expected for stacked CT complexes. The $\omega = 0$ component of the four-spin correlation $\langle S_i^z(t) S_{i+1}^z(t) S_{i+1}^z(0) S_i^z(0) \rangle$ is in qualitative agreement with the Carboni-Richards[8] calculation for finite linear chains.

There are other $Cu(NH_3)_4^{++}$ crystals with magnetically equivalent CT complexes[12] and there are undoubtedly many other copper crystals with magnetically equivalent sites. But previous careful linewidth studies, for example in $Cu(NH_3)_4SO_4 \cdot H_2O$ (CTS)[13] and in $K_2CuCl_4 \cdot 2H_2O$,[14] were on crystals with two inequivalent sites and were restricted to a few orientations of the external field $\vec{H}_0$ at which the Larmor frequencies were equal. While such complications can be treated theoretically,[15] it is clearly advantageous to study spin dynamics first in systems such as CTP or TMMC,[10] with the maximum simplicity.

A second advantage of CTP is the occurrence of a diamagnetic $PtCl_4^{--}$ complex between successive CT's, as seen in the crystal structure[16] shown schematically in Fig. 1. The $PtCl_4^{--}$ complexes provide a degree of magnetic dilution and lead to comparable hyperfine and dipolar local fields. The

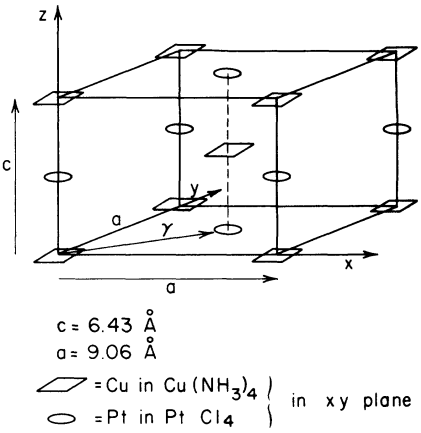

FIG. 1. Schematic representation of the CTP crystal lattice; the tetragonal c axis is the crystal-needle axis.

analysis of the hyperfine interaction requires almost exclusively the two-spin autocorrelation function $C(t)$ and is consequently straightforward. Dipolar fields, by contrast, lead to the far more complicated four-spin correlation functions.

A third advantage of CTP is that the exchange falls conveniently between the standard X- and Q-band frequencies. Our experiments provide the first detailed angular study of the "10/3" effect[5,13,14] named after the $\frac{10}{3}$ linewidth ratio expected in an isotropic powder when the Larmor frequency ω_0 is, respectively, much smaller and much larger than $J_{ij}/\hbar$. Previous "10/3" studies in CTS[13] pointed to one-dimensional exchange, while those in $K_2CuCl_4 \cdot 2H_2O$[14] must be reinterpreted in view of the unexpected temperature dependence.[17] The angular dependence of the "10/3" effect in CTP pro-

TABLE I. Local fields in $Cu(NH_3)_4PtCl_4$ (10^{-3} G^2).

Direction of $\vec{H}_0$	Dipolar second moment[a]				Hyperfine second moment[b]	
	secular		nonsecular			
θ[c]	intrachain	interchain	$\Delta m = \pm 1$	$\Delta m = \pm 2$	secular	nonsecular
$\hat{\gamma}$	6.7	23.5	20.1	16.3	2.0	28.6
60° (γc)	0.5	21.2	30.1	13.8	16.9	21.1
45° (γc)	1.7	18.5	36.6	13.0	30.6	14.3
30° (γc)	10.7	11.1	34.0	12.9	43.3	7.9
$\hat{c}$	26.8	5.9	28.2	12.2	55.1	2.0
30° (ac)	10.7	11.1	35.2	11.6	43.3	7.9
45° (ac)	1.7	14.3	41.2	12.5	30.6	14.3
60° (ac)	0.5	12.5	38.9	13.4	16.9	21.1
$\hat{a}$	6.7	6.9	38.5	14.5	2.0	28.6

[a] $g = 2.11$ and spins quantized along $g\vec{H}_0$.
[b] $g_{\parallel} = 2.216$, $g_{\perp} = 2.050$; $A_{\parallel} = 210G$, $A_{\perp} = 40$ G.
[c] θ is the azimuthal angle in the γc plane (γc) or in the ac plane (ac).

vides strong evidence that, at least for high frequencies, the diagonal four-spin correlation functions are adequately represented by the Fourier components of $C^2(t)$.

The paper is organized as follows. The width of the exchange-narrowed Lorentzian EPR line in CTP is the principal experimental data presented in Sec. II and shown in Figs. 2 and 3. The linewidth is analyzed in Sec. III in terms of hyperfine and dipolar local fields, whose amplitudes are summarized in Table I. The angular dependence of the "10/3" effect is used in Sec. IV to obtain the nonsecular components of the spin correlations. The secular ($\omega = 0$) Fourier components are then obtained and interpreted in terms of one-dimensional exchange along the CT stacks, and the results are compared with several choices for $C(t)$.

II. EPR OF CTP

Deep-purple needles (maximum size about 3×0.2 mm) of CTP were prepared by diffusing dilute aqueous solutions of K_2PtCl_4 (0.10 g in 5 ml of H_2O) and $Cu(NH_3)_4SO_4$ (0.06 g in 4 ml of H_2O plus 1 ml of concentrated NH_4OH) at 4 °C for 5 days into opposite ends of a 12-cm tube containing 11 ml H_2O. The crystal structure[16] of CTP indicates infinite alternating stacks of square planar CT and $PtCl_4^{--}$ complexes, as shown in Fig. 1, and the long axis of the tetragonal prisms is the needle axis. The paramagnetism is associated with the $3d^9$ configuration of Cu^{++} and, for a square planar complex, the unpaired electron is primarily in the $d_{x^2-y^2}$ orbital. As shown in Fig. 1, all the CT complexes are in the xy plane perpendicular to the needle axis. The CT and $PtCl_4^{--}$ complexes thus form interpenetrating body-centered tetragonal lattices.

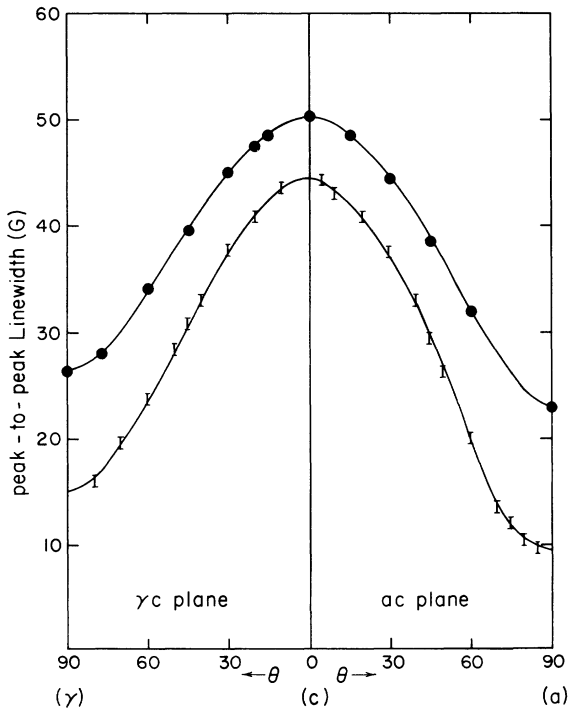

FIG. 2. Peak-to-peak derivative EPR linewidth in CTP at room temperature for $\vec{H}_0$ in the ac and γc planes at X band (●) and at Q band (I).

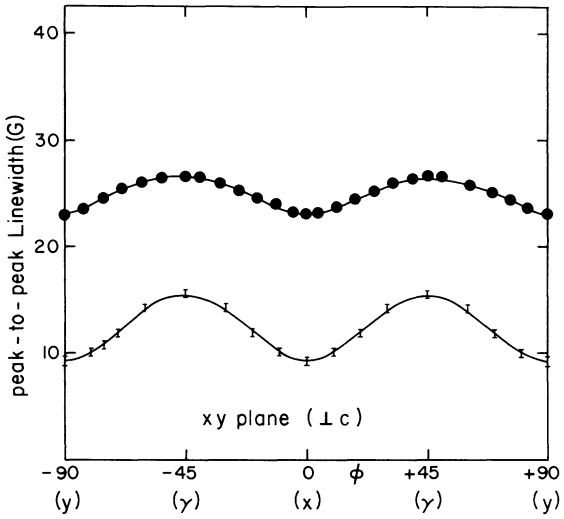

FIG. 3. Peak-to-peak derivative EPR linewidth in CTP at room temperature for $\vec{H}_0$ in the xy plane at X band (●) and at Q band (I).

All EPR spectra were taken with a standard Varian X-band (9.5-GHz) or Q-band (35-GHz) bridge at 100-kHz modulation. A single absorption was observed for any orientation of $\vec{H}_0$, and the line was completely Lorentzian to at least five linewidths, the experimental limit for single scans. Particular attention was given to the shape of the Q band line for $\vec{H}_0 \| \hat{c}$, where the interchain secular linewidth is small and nonsecular terms are suppressed by the large ω_0. The cavity was purged with a steady flow of N_2 gas to remove asymmetries due to O_2 resonances. A more direct comparison with theory (cf. Fig. 2 of Ref. 10) is given by the shape of the absorption $I(\omega)$ rather than the derivative $I'(\omega)$. Since the CTP samples were too small to observe $I(\omega)$ directly with good signal-to-noise ratio, $I'(\omega)$ was recorded directly on a Fabritek signal averager, averaged to good signal-to-noise ratio and symmetry and then integrated in the Fabritek. Good absorption line shapes were obtained and were found to deviate negligibly from a Lorentzian. For example, at three half-widths from the center, a Lorentzian $I(\omega)$ is down by a factor of 10 from $I(0)$, TMMC is down by a factor of 25 [as expected[10] for $I(\omega)$ between Lorentzian and Gaussian], and a Gaussian is down by about 500. CTP is down

by 12 ± 1 and the deviation is even smaller closer to the center of the line. Thus the absorption in CTP is Lorentzian to within the experimental error. The extreme simplicity of a one-line spectrum was essential to establish Lorentzian behavior far into the wings.

The X-band EPR spectra were unchanged at liquid N_2, and a 120 °K run at Q band also failed to change the linewidth. A Weiss constant of 13 °K has been estimated[18] for CTP from susceptibility data down to 77 °K, and lower temperature χ data[19] require a smaller Weiss constant by about an order of magnitude. A Weiss constant[19] of about $\frac{1}{2}$ °K is consistent with a nearest-neighbor exchange of about 5000 G in CTP, and thus with the J values deduced below from the EPR linewidth. It should be noted, however, that the Weiss constant is a preliminary estimate[19] and, further, that it can be related quantitatively to the exchange parameters $J_{ij} = J(r_{ij})$ only if their distance dependence is known. The high-temperature limit ($kT \gg J$) was thus expected to hold for CTP at both 300 and 77 °K and the low-temperature results were primarily to rule out any anomalous effects as observed in $K_2CuCl_4 \cdot 2H_2O$.[17]

The coincidence of the CTP needle axis, of the crystallographic tetragonal axis,[16] and of the CT g-tensor principal axes greatly simplified orienting the crystal in the applied field $\vec{H}_0$. Room-temperature peak-to-peak derivative linewidths at X and Q band are shown in Fig. 2 for $\vec{H}_0$ in the ac and γc planes defined in Fig. 1. The linewidth anisotropy in the xy plane, where the position of the line is constant at $g_\perp$, is shown in Fig. 3 for both X and Q band.

Since all the $S = \frac{1}{2}$ CT complexes are magnetically equivalent, the Zeeman interaction reduces to

$$\mathcal{H}_Z = \mu_B \vec{H}_0 \cdot \sum_i \vec{\vec{g}}_i \cdot \vec{S}_i = \mu_B \vec{H}_0 \cdot \vec{\vec{g}} \cdot \vec{s} , \tag{5}$$

where μ_B is the Bohr magneton, $\vec{H}_0$ is the applied static field, and $\vec{s} = \sum_i \vec{S}_i$ is the total electronic spin. The Larmor frequency ω_0 for $\vec{H}_0 = H_0(\sin\theta\cos\varphi, \sin\theta\sin\varphi, \cos\theta)$ is axially symmetric for square-planar CT complexes

$$\hbar\omega_0(\theta) = \mu_B H_0 g(\theta) = \mu_B H_0 (g_\parallel^2 \cos^2\theta + g_\perp^2 \sin^2\theta)^{1/2} . \tag{6}$$

The position of the EPR line leads to $g_\parallel = 2.22 \pm 0.01$ and $g_\perp = 2.05 \pm 0.01$ and to principal g-tensor axes that coincide with the crystallographic unit cell axes. The g values are in complete agreement with previous CT studies.[12,20]

III. EXCHANGE NARROWED LINEWIDTH

The general theories of magnetic resonance[5,9] in exchange-coupled systems start with a zeroth-order Hamiltonian

$$\mathcal{H}_0 = \mathcal{H}_Z + \mathcal{H}_e \tag{7}$$

consisting of the Zeeman interaction (5) and the exchange interaction (1). Although the Larmor frequency $\omega_0(\theta)$ in (6) depends on the orientation of the external field, all the CT complexes in CTP have the same Larmor frequency and $\mathcal{H}_Z$ is simply proportional to a component of the total spin. The resonance absorption $I(\omega - \omega_0)$ is then given by[5,9]

$$I(\omega - \omega_0) = (1/2\pi) \int_{-\infty}^{\infty} dt\, \varphi(t)\, e^{i(\omega - \omega_0)t} . \tag{8}$$

$\varphi(t)$ is the correlation function for the decay of the transverse magnetization

$$\varphi(t) = \exp\left[- \int_0^t (t - \tau)\, \psi(\tau)\, d\tau \right] . \tag{9}$$

Local dipolar and hyperfine fields are taken as perturbations to $\mathcal{H}_0$ and lead to small deviations $\Delta\omega$ from ω_0, with $\Delta\omega \ll \omega_0$. The local-field correlation function[5,9,21]

$$\psi(\tau) = \langle \Delta\omega(\tau)\, \Delta\omega(0) \rangle \tag{10}$$

is the basic quantity to be computed. Its magnitude $\psi(0)$ is given by the second-frequency moment. Its time dependence is governed by $\mathcal{H}_Z + \mathcal{H}_e$, but the Zeeman contribution can readily be treated exactly and leads to the familiar secular and nonsecular contributions.[5]

Exchange narrowing occurs if $\psi(\tau)$ decays rapidly in comparison to the times of interest in $\varphi(t)$. When the stronger approximation

$$\varphi(t) \approx \varphi_0(t) = \exp\left[- t \int_0^\infty \psi(\tau)\, d\tau \right] \tag{11}$$

holds, a peak-to-peak derivative width ΔH and half-width at half-power Γ is obtained from (8) with

$$\tfrac{1}{2}\sqrt{3}\,\Delta H = \Gamma = \int_0^\infty \psi(\tau)\, d\tau . \tag{12}$$

The approximation (11) requires that τ, of the order of $\hbar/J$, be much less than Γ^{-1}, the times of interest in $\varphi(t)$. It also requires that $\psi(\tau)$ be integrable, which is not the case, for example, in one-dimensional[10,11] spin diffusion, when $\psi(\tau) \propto \tau^{-1/2}$.

The expression (12) for Γ is basic to the analysis of the CTP linewidth data summarized in Figs. 2 and 3. For one-dimensional motion, when (11) fails, deviations from Lorentzian behavior are expected[22] and observed in TMMC[10] and several Cu systems.[11] The best chance for observing non-Lorentzian behavior in CTP is at Q band with $\vec{H}_0$ along the c axis. There the secular dipolar interactions are almost entirely due to spins in the same stack, while the nonsecular interchain contributions are suppressed for $\omega_0 > J/\hbar$. No deviations from Lorentzian behavior were observed to about seven linewidths, the experimental limit. As has been shown[23] for several nearly one-dimensional systems, very small interchain interactions are sufficient to suppress the deviations and to give a Lorentzian exchange-narrowed line. Thus, the approximation (11) is consistent with the CTP data.

A. Hyperfine Field

The local-field correlation $\psi(\tau)$ contains both dipolar and hyperfine contributions. We begin with the hyperfine contribution, where $\psi(\tau)$ is simply proportional to $C(\tau)$ in the absence of transfer hyperfine terms.[21] The hyperfine interaction between the unpaired electron and the $I=\frac{3}{2}$ Cu nucleus, for either ^{63}Cu or ^{65}Cu, is

$$\mathcal{H}_h=\sum_i \vec{I}_i\cdot\vec{\vec{A}}\cdot\vec{S}_i \quad . \tag{13}$$

The principal axes of the hyperfine tensor coincide with the g tensor and are, respectively, $A_\perp$, $A_\perp$, $A_\parallel$ in the x, y, z coordinates of Fig. 1. Typical values for CT are $A_\parallel=210$ G and $A_\perp=30$ G.[24] Fritz and Keller[20] doped CT into the isomorphous MGS lattice and report $A_\parallel=225$ G, $A_\perp=30$ G, without presenting details of either their data or analysis. We have used $A_\parallel=210$ G, $A_\perp=40$ G in computing the hyperfine second moments in Table I. The larger $A_\perp$ value represents in part the small but observable $I=1$ nitrogen hyperfine of a CT complex.[20] The hyperfine field in the approximation (12) has full axial symmetry about the tetragonal (need'e) axis.

Neglecting the slow nuclear spin relaxation, we obtain

$$\Gamma_h=\int_0^\infty (a^{(0)}+a^{(1)}\cos\omega_0 t)\,C(t)\,dt \tag{14}$$

for the linewidth contribution of the hyperfine interaction. The time evolution due to $\mathcal{H}_Z$ is contained in the $\cos\omega_0 t$ coefficient of the nonsecular term. The secular and nonsecular contributions $a^{(0)}$ and $a^{(1)}$ represent, respectively, hyperfine fields parallel and perpendicular to the effective field $g\vec{H}_0$ along which the electronic spins are quantized. The high-temperature second moments $a^{(0)}$ and $a^{(1)}$ for axially symmetric g and A tensors with collinear principal axes are[25]

$$a^{(0)}=\tfrac{5}{4}K^2(\theta)/g^2(\theta) \quad , \tag{15}$$

$$a^{(1)}=\tfrac{5}{8}[A_\parallel^2A_\perp^2/g^2(\theta)+A_\perp^2+E^2(\theta)] \tag{16}$$

for spin $I=\frac{3}{2}$; $g(\theta)$ is given in (6), while

$$K^2(\theta)=A_\parallel^2g_\parallel^2\cos^2\theta+g_\perp^2A_\perp^2\sin^2\theta \quad , \tag{17}$$

$$E(\theta)=(A_\perp^2-A_\parallel^2)g_\parallel g_\perp\sin\theta\cos\theta/K(\theta)g^2(\theta) \quad . \tag{18}$$

Except for $\theta=0$ and $\frac{1}{2}\pi$, $\vec{H}_0$ is not parallel to $g\vec{H}_0$ and it is important to use the complete expressions (15) and (16) for computing the second moments $a^{(0)}$ and $a^{(1)}$ listed in Table I.

In the high-temperature limit, $C(t)$ is an even function[7] and Γ_h reduces to

$$\Gamma_h=a^{(0)}g(0)+a^{(1)}g(\omega_0) \quad , \tag{19}$$

where $g(\omega)$ are Fourier components of the autocorrelation function

$$2g(\omega)=\int_{-\infty}^{\infty}e^{i\omega t}\,C(t)\,dt \quad . \tag{20}$$

The Larmor frequency ω_0 is experimentally fixed, while the magnitude of H_0, with H_0 much larger than either the dipolar or hyperfine fields, is varied to satisfy the resonance condition (6). X- and Q-band EPR data thus provide the 9.47- and 34.9-GHz Fourier components, respectively, as well as the secular component at $\omega=0$.

B. Dipolar Fields

Since electron dipolar interactions usually dominate in paramagnetic crystals, the dipolar contributions to $\psi(\tau)$ and to the linewidth Γ have been analyzed in detail.[5,25] We follow here the treatment of both secular and nonsecular contributions given by Carboni and Richards,[8] and focus attention on the approximations that lead to the familiar Van Vleck[26] second moments.[5,25]

Dipolar interactions between point dipoles lead to four-spin correlation functions[8] for $\psi(\tau)$,

$$C_{ijkl}(t)=\left(\frac{3}{2S(S+1)}\right)^2\langle S_i^+(t)S_j^+(t)S_k^-(0)S_l^-(0)\rangle \quad , \tag{21}$$

where i, j, k, l refers to various CT sites in the crystal and $i\neq j$, $k\neq l$. In the high-temperature limit of uncorrelated spins, the $t=0$ result is

$$[3/2\,S(S+1)]\langle S_i^+(0)S_k^-(0)\rangle=\delta_{ik} \quad . \tag{22}$$

Using this result for $t>0$ in (21) restricts $C_{ijkl}(t)$ to diagonal correlations of the form $C_{ijij}(t)$ or $C_{ijji}(t)$, whose dipolar coefficients are just the terms in the usual second moment expressions.[5,8,25] The secular contribution for $S=\frac{1}{2}$ is

$$M_2^{(0)}=\frac{9\bar{g}^4(\mu_B)^4}{16\hbar^2}\sum_{j\neq i}(3\cos^2\psi_{ij}-1)^2r_{ij}^{-6} \quad , \tag{23}$$

where the sum is the same for any CT site i in CTP, $\bar{g}=2.11$ is the average g value, and ψ_{ij} is the angle between $\vec{r}_{ij}$ and the effective field $g\vec{H}_0$. For an orientation (θ,φ) of $\vec{H}_0$, the effective field angles (ψ,φ) are

$$\cos\psi=[g_\parallel/g(\theta)]\cos\theta \quad . \tag{24}$$

Thus $g\vec{H}_0$ and $\vec{H}_0$ are parallel for $\theta=0$ and $\frac{1}{2}\pi$, when (23) reduces to the usual expression[8] involving the angle between $\vec{H}_0$ and $\vec{r}_{ij}$. The corresponding second moment for $\Delta m=\pm1$ transitions is

$$M_2^{(1)}=\frac{90\bar{g}^4(\mu_B)^4}{16\hbar}\sum_{j\neq i}r_{ij}^{-6}\sin^2\psi_{ij}\cos^2\psi_{ij} \tag{25}$$

and for $\Delta m=\pm2$ transitions,

$$\Delta M_2^{(2)}=\frac{9\bar{g}^4(\mu_B)^4}{16\hbar^2}\sum_{j\neq i}r_{ij}^{-6}\sin^4\psi_{ij} \quad . \tag{26}$$

The various dipolar second moments are listed in Table I for $\bar{g}=2.11$, with $M_2^{(0)}$ further separated into contributions from CT complexes in the same

and in different stacks.

The dipolar entries in Table I contain several approximations beyond the restriction to diagonal four-spin correlations. It is of course straightforward[27,28] to retain $g_{\parallel}$ and $g_{\perp}$ explicitly, and the complete analysis never changes the $\bar{g}$ plus effective field $g\vec{H}_0$ result by more than a few percent.[28] The complete (secular and nonsecular) dipolar second moment retains its axial symmetry about $\hat{c}$. Except for the small nitrogen hyperfine,[20] the CTP linewidth is thus axially symmetric for $\omega_0 \ll J/\hbar$ and the smaller xy anisotropy at X band shown in Fig. 3 is expected. The point dipole approximation for (23), (25), and (26) can introduce 5% errors, since the unpaired electron is largely in a nonspherical $d_{x^2-y^2}$ Cu orbital. The actual electron distribution must eventually be reflected in the dipolar second moments, as in the case of fully delocalized π electron in organic solids.[2,29]

We now multiply each term in $M_2^{(0)}$, $M_2^{(1)}$, and $M_2^{(2)}$ by the appropriate diagonal four-spin correlation function $C_{iji}(t)$. Then we substitute into (12) to obtain the dipolar contribution to the linewidth. Finally, we use the high-temperature limit to obtain the 0, ω_0, and $2\omega_0$ Fourier components of $C_{iji}(t)$. Each diagonal $C_{iji}(t)$ contains, in the most approximate decoupling, the square of the autocorrelation function,

$$\langle S_i^+(t)S_j^+(t)S_i^-(0)S_j^-(0)\rangle \approx \langle S_i^+(t)S_i^-(0)\rangle^2 \propto C^2(t) \ , \quad (27)$$

which is independent of the site index i. The dipolar linewidth then reduces to

$$\Gamma d = (M_2^{(0)} - M_2')f(0) + M_2' f_1(0) + M_2^{(1)} f(\omega_0) + M_2^{(2)} f(2\omega_0) \ , \quad (28)$$

where $f(\omega)$ is a Fourier component of $C^2(t)$,

$$2f(\omega) = \int_{-\infty}^{\infty} C^2(t)\, e^{i\omega t}\, dt \ . \quad (29)$$

We have retained in (28) the possibility of different intrachain secular contributions, denoted by $M_2' f_1(0)$. As already mentioned, the analysis of dipolar linewidths is complicated by the occurrence of a variety of four-spin correlations,[8] $C_{ijkl}(t)$, all with potentially different Fourier components. The diagonal correlations $C_{iji}(t)$ in CTP can be analyzed in terms of $j = i + (0,\ 0,\ \pm c)$ in Fig. 1 for nearest-neighbor intrachain correlations, with Fourier components $f_1(\omega)$ related to the transform of $\langle S_i^+(t)S_{i+1}^+(t)S_{i+1}^-(0)S_i^-(0)\rangle$. The eight second-neighbor interchain diagonal correlations arise for $j = i + (\pm\frac{1}{2}a,\ \pm\frac{1}{2}a,\ \pm\frac{1}{2}c)$ in $C_{iji}(t)$. Their Fourier coefficients are approximated by $f(\omega)$ in (29), since we expect largely intrachain exchange in CTP and, for spins in different chains, the strong decoupling (27) is exact for vanishing interchain exchange.

We approximate diagonal correlations for more distant neighbors by $f(\omega)$ as well and further assume that $f_1(\omega) = f(\omega)$ for $\omega \neq 0$. While it is plausible that corrections to the decoupling (27) should be largest near $\omega = 0$, where the long-time behavior is important, our present motivation is to retain the fewest number of adjustable parameters in (28). In particular, the observed CTP linewidths are given below to within experimental error with only four dipolar Fourier components: $f(0)$ and $f_1(0)$ for interchain and intrachain secular components and $f(\omega_0)$, $f(2\omega_0)$ for nonsecular components. Thus, we cannot extract corrections to the strong decoupling (27) for $\omega \neq 0$ from the present data. Neither can our results justify introducing for $\omega \neq 0$ any nondiagonal four-spin correlations, which vanish exactly only at $t = 0$ according to (22). Their contributions vanish in strong decoupling, but are comparable to the corrections to (27) and must be included in more accurate treatments. To our knowledge, the present work provides the first experimental demonstration that two different secular components $f(0)$ and $f_1(0)$ must be used for interchain and intrachain correlations.

IV. SPIN CORRELATION FUNCTIONS

The X- and Q-band CTP linewidths in Figs. 2 and 3 are summarized in Table II. The dipolar and hyperfine second moments in Table I contribute to the linewidth Γ as indicated in (28) and (19). The angular dependence of Γ thus provides equations in which the Fourier components $g(0)$, $g(\omega)$, $f(0)$, $f_1(0)$, $f(\omega)$, and $f(2\omega)$ are the only unknowns. A consistent solution for these coefficients indicates that, to experimental accuracy, the strong decoupling (27) is adequate for $\omega \neq 0$.

We first examine the nonsecular ($\omega \neq 0$) contribu-

TABLE II. Experimental and calculated peak-to-peak linewidths (G).

Orientation of $\vec{H}_0$ θ[a]	X band Expt. (±1 G)	Calc.[b]	Q band Expt. (±1 G)	Calc.[b]
$\hat{\gamma}$	23.1	22.9	13.4	13.6
60° (γc)	29.4	28.6	20.3	19.7
45° (γc)	34.2	34.9	26.8	26.5
30° (γc)	39.0	39.1	32.4	32.2
$\hat{c}$	43.8	44.8	38.5	39.6
30° (ac)	38.5	39.2	32.3	32.2
45° (ac)	34.1	23.9	25.5	25.0
60° (ac)	27.7	26.6	17.3	16.5
$\hat{a}$	19.9	18.8	8.2	7.4

[a] θ is the azimuthal angle in the γc plane (γc) or in the ac plane (ac).

[b] With $\hat{J} = 7400$ G in $C_{BH}(t)$ (31) and $g(0) = 0.55 \times 10^{-3}$ G^{-1}, $f(0) = 0.42 \times 10^{-3}$ G^{-1}, $f_1(0) = 0.22 \times 10^{-3}$ G^{-1} as explained in text.

tions to the linewidth by taking the difference of the X- and Q-band results. The approximation (22) of neglecting off-diagonal $C_{ij}(t)$ fails at long t, or small ω, since spin diffusion requires[7,8,21] that $C_{ii+1}(t)$ eventually be comparable to $C_{ii}(t)$. The stacking of the CT complexes in CTP suggests one-dimensional superexchange through the $PtCl_4^{--}$. One-dimensional anomalies[8,10] with $\psi(t)$ are again worst at long t, or small ω, and the divergence of $g(0)$[30] and of $f(0)$[24] have been demonstrated for purely one-dimensional exchange between $S=\frac{1}{2}$ sites.

A. Nonsecular Linewidth

The difference between the X- and Q-band linewidth for various orientations (θ,φ) of H_0 leads, from (12), (19), and (28), to

$$\tfrac{1}{2}\sqrt{3}[\Delta H^{(X)}(\theta,\varphi)-\Delta H^{(Q)}(\theta,\varphi)] = M_2^{(1)}(\theta,\varphi)\Delta f(\omega) + M_2^{(2)}(\theta,\varphi)\Delta f(2\omega)+a^{(1)}(\theta)\Delta g(\omega)\ , \quad (30)$$

where $\Delta f(\omega)=f(\omega_X)-f(\omega_Q)$ is the difference in the X- and Q-band Fourier components and $\Delta f(2\omega)$ and $\Delta g(\omega)$ are the corresponding differences at twice the Larmor frequency and for the hyperfine local field, respectively. The hyperfine second moment $a^{(1)}$ is axially symmetric if the nitrogen splittings are neglected. The Fourier components $\Delta f(\omega)$, $\Delta f(2\omega)$, and $\Delta g(\omega)$ describe the time evolution due solely to $\mathcal{H}_e$ and are independent of the orientation of $\vec{H}_0$. The Fourier components at $\omega_X=9.47$ GHz and $\omega_Q=34.9$ GHz enter in (30) for any orientation of $\vec{H}_0$, whose magnitude for fixed ω_0 varies as indicated in (6).

The difference equations (30) are solved to within the ± 1 G experimental accuracy by $\Delta f(\omega)=0.12\times10^{-3}$ G^{-1}, $\Delta f(2\omega)=0.10\times10^{-3}$ G^{-1}, and $\Delta g(\omega)=0.18\times10^{-3}$ G^{-1}. The uncertainty is about 10% if corresponding changes increasing and decreasing different Fourier components are made. Since very different four-spin correlations contribute for different orientations of $\vec{H}_0$, the fitting of the angular dependence of the "10/3" effect by just two dipolar Fourier components indicates that, at least at high frequencies, the strong decoupling (27) is justified. On the other hand, once strong decoupling is established, then any assumed form for the autocorrelation $C(t)$ provides not only $\Delta g(\omega)$ but, through the Fourier components of $C^2(t)$, the values of $\Delta f(\omega)$ and $\Delta f(2\omega)$ as well. In Fig. 4 the observed angular variation of the "10/3" effect is compared with a one-parameter form for $C(t)$ due to Blume and Hubbard[7] given below. A similarly good fit follows from a one-parameter Gaussian $C(t)$ proposed by Anderson and Weiss,[9] while an exponential $C(t)$ cannot fit the difference equations.

The Blume-Hubbard high-temperature approxi-

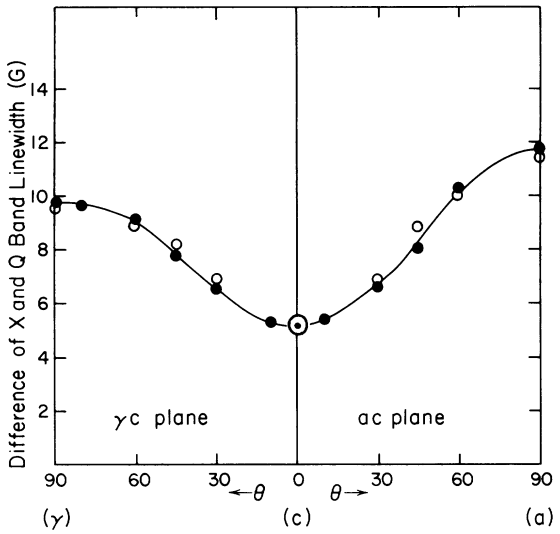

FIG. 4. Angular variation of the difference between the X- and Q-band linewidths (●) in CTP at room temperature for $\vec{H}_0$ in the ac and γc planes; the theoretical results (O) are based on $C_{BH}(t)$ given in (31), with $\hat{J}=7400$ G, as discussed in the text.

mation for $C(t)$ for $S=\frac{1}{2}$ is[7]

$$C_{BH}(t)=\cosh^{-2}(\tfrac{1}{2}\hat{J}t)\ , \quad (31)$$

where $\hat{J}$ is the root-mean-square exchange at a site

$$\hat{J}^2=\sum_j J_{ij}^2 \quad (32)$$

and is the adjustable parameter of the model. The analytical expression (31) is a good approximation, except at long t, to a numerical analysis and also to Windsor's[6] result for classical spins. The Fourier components (20) of $C_{BH}(t)$ give

$$g_{BH}(x)=(2/\hat{J})x/\sinh x\ , \quad (33)$$

where $x=\pi\omega/\hat{J}$; the components (29) of $C_{BH}^2(t)$ are

$$f_{BH}(x)=\frac{4}{3\hat{J}}\ \frac{x}{\sinh x}\left[1+\left(\frac{x}{\pi}\right)^2\right]. \quad (34)$$

For $\hat{J}=7400$ G, with $\omega_X=9.47$ GHz and $\omega_Q=34.9$ GHz, we have $g(\omega_X)=0.195\times10^{-3}$ G^{-1}, $g(\omega_Q)=0.015\times10^{-3}$ G^{-1}; $f(\omega_X)=0.158\times10^{-3}$ G^{-1}; $f(\omega_Q)=0.037\times10^{-3}$ G^{-1}; $f(2\omega_X)=0.110\times10^{-3}$ G^{-1}; $f(2\omega_Q)=0.0013\times10^{-3}$ G^{-1}. The anisotropy of the "10/3" effect is quantitatively reproduced, as shown in Fig. 4. The fit is noticeably poorer for a ± 500-G change in $\hat{J}$.

The Anderson-Weiss[9] proposal of Gaussian $C(t)$ for exchange narrowing

$$C_G(t)=\exp(-\tfrac{1}{4}\pi\omega_e^2t^2)\ , \quad (35)$$

with $\omega_e\sim J$ the adjustable parameter, leads to virtually the same ω_X and ω_Q Fourier components for $\omega_e\simeq 4100$ G. It of course decays more rapidly at large ω than the Blume-Hubbard function, but the linewidth contributions there are small. On the

other hand, we can rule out an exponential $C(t)$,

$$C_e(t) = e^{-\omega_m t} \quad , \tag{36}$$

by observing that $g_e(\omega) = \omega_m/(\omega_m^2+\omega^2)$ has a maximum of $(2\omega)^{-1}$ as a function of ω_m. At X band, $g_e(\omega)$ must thus be smaller than $[2\times(3380\ \mathrm{G})]^{-1} \sim 0.147\times10^{-3}\ \mathrm{G}^{-1}$. Any Q-band contribution leads to even smaller Δg and cannot fit the value of $0.18 \times10^{-3}\ \mathrm{G}^{-1}$ obtained from the difference equations. Thus, $C_e(t)$ is unacceptable for any ω_m. Other choices[8,21] for $C(t)$ can be tested in the same way.

The more slowly decaying exponential $C_e(t)$ leads to a stronger $\omega = 0$ peak in $g(\omega)$ and, as such, has been used[13,31] as a first approximation for the one-dimensional anomalies associated with the divergence[30] of $g(0)$ and of $f(0)$, even though $C_e(t)$ has an incorrect short time form. In the present method, the angular dependence of the linewidth permits a direct evaluation of the nonsecular contributions at X and Q band, without dealing with the secular components. The short-time behavior of $C(t)$, which dominates in the high-frequency components, is rather similar for three-dimensional[7,9] and one-dimensional[8] exchange (see Fig. 8 of Ref. 8 and Fig. 1 of Ref. 7).

B. Secular Linewidth

The over-all fit of the CTP linewidth at X and Q band shown in Table II is based on $\hat{J} = 7400$ G in $C_{\mathrm{BH}}(t)$ for the $\omega \neq 0$ Fourier components and on three secular parameters: $g(0) = 0.55\times10^{-3}\ \mathrm{G}^{-1}$, $f(0) = 0.42\times10^{-3}\ \mathrm{G}^{-1}$, and an intrachain component $f_1(0) = 0.22\times10^{-3}\ \mathrm{G}^{-1}$. Again, the wealth of angular data, with very different mixes of hyperfine, interchain and intrachain local fields, provides sufficient equations for fitting three secular parameters. We estimate that $g(0)$ and $f(0)$ are accurate to better than 5%, while $f_1(0)$ is only accurate to about 10%, excluding the numerical approximations in the second moments discussed in Sec. III B.

The nonsecular X- and Q-band Fourier components based on $C_{\mathrm{BH}}(t)$ or $C_G(t)$ lead to consistent estimates for the secular linewidth. But the secular contributions cannot be obtained from $C_{\mathrm{BH}}(t)$, which for $\hat{J} = 7400$ G leads to $g(0) = 0.27\times10^{-3}\ \mathrm{G}^{-1}$ and $f(0) = 0.18\times10^{-3}\ \mathrm{G}^{-1}$. [A 10% larger value for $g(0)$ is found numerically[7] for a $C(t)$ which decreases less rapidly at long t than (31).] The $\omega = 0$ result for $C_G(t)$ and $\omega_e = 4100$ G is even worse, as expected from the more rapid decrease at long t. The approximation of diagonal four-spin correlations is worst at long t, where (22) does not hold and $C_{ii+1}(t) \approx C_{ii}(t)$; the strong decoupling (27) is also probably worse[8] at long t. The corrections tend to increase the dipolar coefficients, and thus to decrease $f(0)$. A factor of 2 decrease in $f(0)$ is unexpected, however, and is even more surprising for $g(0)$ obtained from the hyperfine broadening. We believe that the large $\omega = 0$ components reflect the one-dimensional exchange suggested by the stacking of $Cu(NH_3)_4^{++}$ and $PtCl_4^{--}$ complexes in CTP.

As already mentioned, the observation of a Lorentzian line, even at Q band along the c axis, precludes a purely one-dimensional exchange, but is consistent with rather weak interchain interactions.[23] The $\omega^{-1/2}$ divergence of $g(0)$ and the logarithmic divergence of $f(0)$ is suppressed, presumably by interchain exchange. The Fourier transform of the intrachain four-spin correlation $\langle S_i^z(t)S_{i+1}^z(t)S_{i+1}^z(0)S_i^z(0)\rangle$ may not diverge even in the one-dimensional limit.[24] The exchange constant J used by Carboni and Richards[8] is $\hat{J}/2\sqrt{2} \simeq 2600$ G for linear chains. The numerical result[24] for the intrachain correlations, which correspond to $f_1(0)$, leads to $0.36\times10^{-3}\ \mathrm{G}^{-1}$. The experimental value of $f_1(0) = 0.22\times10^{-3}\ \mathrm{G}^{-1}$ is consistent with less than perfect one-dimensional exchange in CTP. It should be noted that the interchain experimental value of $f(0) = 0.42\times10^{-3}\ \mathrm{G}^{-1}$, which for one-dimensional exchange diverges, is larger than $0.36\times10^{-3}\ \mathrm{G}^{-1}$. Strong decoupling (27) becomes exact[23] for interchain dipolar correlations if there is no interchain exchange. Since interchain dipolar contributions are usually more than half of the total dipolar second moment, the success of the strong decoupling approximation for the nonsecular components is also consistent with largely one-dimensional exchange.

The anomalously large secular components $g(0)$ and $f(0)$ could be fit with, for example, a two-parameter choice of $C(t)$ in which the long-t behavior is allowed to decrease much more slowly. The main conclusion from the experimental results for $g(0)$, $f(0)$ and for $g(\omega)$, $f(\omega)$, $f(2\omega)$ at $\omega = \omega_X$ and ω_Q is that, except near $\omega = 0$, the largely one-dimensional exchange does not affect the spin correlations. This is consistent with the similar theoretical short time results for $C(t)$ in one- and three-dimensional cases.[7,8] Thus, only long-time corrections to $C_{\mathrm{BH}}(t)$, for example, are required rather than completely different guesses such as $C_e(t)$.

C. Summary

We have shown that, in crystals with magnetically equivalent sites, the angular dependence of the exchange-narrowed Lorentzian EPR line provides a simple direct method for evaluating high-temperature Fourier components of spin correlation functions. Since second-moment computations for hyperfine and dipolar local fields are straightforward, the method can be used in any exchange-coupled crystal with magnetically equivalent sites and provides a direct test for various theoretical models of spin correlation functions.

The angular dependence of the EPR linewidth in CTP at X and Q band gave both secular and nonsec-

ular Fourier components. The nonsecular dipolar components were adequately reproduced by using the strong decoupling (27) for the diagonal four-spin correlations. For $\omega = \omega_X$, $2\omega_X$, ω_Q, or $2\omega_Q$, the Fourier components of $C(t)$ and of $C^2(t)$ were sufficient to fit the difference equations (30) between the X- and Q-band linewidth. The computed nonsecular coefficients were then shown to follow from either the Blume-Hubbard[7] model (31) with rms exchange $\hat{J} = 7400$ G or from a Gaussian $C(t)$ with $\omega_e = 4100$ G. The angular dependence of the "10/3" effect shown in Fig. 4 thus confirms the short time analysis[7] of $C(t)$ and rules out an exponential $C_e(t)$.

The secular component showed that specific spin correlations can be evaluated by studying the linewidth anisotropy. Thus, the interchain, or essentially nonexchanging four-spin correlation $f(0) = 0.42\times10^{-3}$ G^{-1} was quite different from $\omega = 0$ component of the intrachain correlation $\langle S_i^x(t)S_{i+1}^x(t)S_{i+1}^x(0)S_i^x(0)\rangle$, which was found to be $f_1(0) = 0.22\times10^{-3}$ G^{-1}. The axial symmetry of both the intrachain and hyperfine correlations in CTP makes it very simple, for example by looking at the linewidth anisotropy in the xy plane as shown in Fig. 3, to isolate purely interchain contributions. The possibility of measuring Fourier components of *specific* spin correlations by the present method is particularly useful, since the difficulty of the theoretical analyses can vary widely. The Fourier component $f_1(0)$ satisfies the Carboni-Richards[8] bound for one-dimensional exchange, while the large values of $g(0)$ and $f(0)$ also suggest largely one-dimensional superexchange through $PtCl_4^{--}$ between successive CT units along the tetragonal axis. We are currently investigating the mechanisms limiting[23] purely one-dimensional behavior in CPT.

ACKNOWLEDGMENTS

We thank M. E. Lines and D. H. Valentine for several discussions and J. S. V. acknowledges financial assistance from the Research Council of Rutgers, the State University.

†Supported in part by NSF-GP-9546 and in part by the U.S. Atomic Energy Commision.

*Alfred P. Sloan Fellow, 1969–1971.

[1]G. F. Kokoszka and G. Gordon, Trans. Metal Chem. 5, 181 (1969); R. L. Martin, in *New Pathways of Inorganic Chemistry*, edited by E. A. V. Ebsworth, A. G. Maddock, and A. G. Sharpe (Cambridge U. P., Cambridge, England, 1968); A. P. Ginzberg, Inorg. Chim. Acta. Rev. 5, 45 (1971); E. Sinn, Coord. Chem. Rev. 5, 313 (1970); N. Kato, H. B. Jonassen, and J. C. Fanning, Chem. Rev. 64, 99 (1964).

[2]P. L. Nordio, Z. G. Soos, and H. M. McConnell, Ann. Rev. Phys. Chem. 17, 237 (1966).

[3]P. W. Anderson, in *Solid State Physics*, edited by F. Seitz and D. Turnbull (Academic, New York, 1963), Vol. 14, pp. 108–14.

[4]W. Marshall and R. D. Lowde, Rep. Progr. Phys. 31, 705 (1968); M. T. Hutchins, G. Shirane, R. J. Birgeneau, and S. L. Holt, Phys. Rev. B 5, 1999 (1972); C. G. Windsor, Proc. Phys. Soc. Lond. 89, 825 (1966).

[5]R. Kubo and K. Tomita, J. Phys. Soc. Jap. 9, 888 (1954); A. Abragam, *The Principals of Nuclear Magnetism* (Clarendon, Oxford, England, 1961), Chaps. IV and X.

[6]C. G. Windsor, Proc. Phys. Soc. Lond. 91, 353 (1967).

[7]M. Blume and J. Hubbard, Phys. Rev. B 1, 3815 (1970). The one-dimensional case has recently been studied by F. B. McLean and M. Blume [Phys. Rev. B 7, 1149 (1973)].

[8]F. Carboni and P. M. Richards, Phys. Rev. 177, 889 (1969).

[9]P. W. Anderson and P. R. Weiss, Rev. Mod. Phys. 25, 269 (1953); P. W. Anderson, J. Phys. Soc. Jap. 9, 316 (1954).

[10]R. E. Dietz, F. R. Merritt, R. Dingle, D. Hone, B. G. Silbernagel, and P. M. Richards, Phys. Rev. Lett. 26, 1186 (1971).

[11]R. R. Bartkowski, M. J. Hennessy, B. Morosin, and P. M. Richards, Solid State Commun. 11, 405 (1972).

[12]A. A. G. Tomlinson, B. J. Hathaway, D. E. Billing, and P. Nichols, J. Chem. Soc. (A) 1969, 66 (1969); B. J. Hathaway and A. A. G. Tomlinson, Coord. Chem. Rev. 5, 1 (1970).

[13]R. N. Rogers, F. Carboni, and P. M. Richards, Phys. Rev. Lett. 19, 1016 (1967).

[14]A. J. Henderson and R. N. Rogers, Phys. Rev. 152, 218 (1966); see also Ref. 17.

[15]M. Yokota and S. Koide, J. Phys. Soc. Jap. 9, 953 (1954).

[16]M. Bukovska and M. A. Porai-Koshitz, Kristallografiya 5, 137 (1960) [Sov. Phys. Cryst. 5, 127 (1960)].

[17]T. A. Kennedy, S. H. Choh, and G. Seidel, Phys. Rev. B 2, 3645 (1970). In addition to the anomalous temperature dependence, a numerical error in Ref. 14 is pointed out, which spoils the apparent agreement for the estimate of J.

[18]J. R. Miller, J. Chem. Soc. Lond. 1961, 4452 (1961).

[19]P. M. Richards (private communication).

[20]H. P. Fritz and H. J. Keller, Z. Naturforsch. B 20, 1145 (1965).

[21]J. E. Gulley, D. Hone, D. J. Scalapino, and B. G. Silbernagel, Phys. Rev. B 1, 1020 (1970).

[22]Z. G. Soos, J. Chem. Phys. 44, 1729 (1966).

[23]M. J. Hennessy, C. D. McElwee, and P. M. Richards, Phys. Rev. B 7, 930 (1973).

[24]C. D. McElwee, Ph. D. thesis (University of Kansas, 1971) (unpublished). A factor of 16π relates $f_1(\omega)$ to the function $\langle S_1^x(t)S_2^x(t)S_2^x(0)S_1^x(0)\rangle$ plotted in Fig. 16, p. 130a. The $A_\parallel$, $A_\perp$ values cited are due to Rogers.

[25]G. E. Pake, *Paramagnetic Resonance* (Benjamin, New York, 1962), pp. 75–89; and 144–150.

[26]J. H. Van Vleck, Phys. Rev. 74, 1168 (1948).

[27]J. F. Boas, R. H. Dunhill, J. R. Pilbrow, R. C. Srivastava, and T. D. Smith, J. Chem. Soc. (A) 1969, 94 (1969).

[28]T. Z. Huang (unpublished).

[29]T. Z. Huang, R. P. Taylor, and Z. G. Soos, Phys. Rev. Lett. 28, 1054 (1972).
[30]J. F. Fernandez and H. A. Gersh, Phys. Rev. 172, 341 (1968); R. A. Tahir-Kheli and D. G. McFadden, Phys. Rev. 178, 800 (1969).
[31]B. M. Hoffman and R. C. Hughes, J. Chem. Phys. 52, 4011 (1970).

PHYSICAL REVIEW B VOLUME 8, NUMBER 3 1 AUGUST 1973

Dechanneling from 2-MeV He^+ Damage in Gold*

K. L. Merkle, P. P. Pronko, D. S. Gemmell,
R. C. Mikkelson,† and J. R. Wrobel
Argonne National Laboratory, Argonne, Illinois 60439
(Received 16 March 1973)

The dechanneling of 2-MeV He^+ incident in the [001] direction of monocrystalline gold films has been investigated by means of the backscattering technique. The aligned spectra of the undamaged crystal indicate good agreement with channeling theories regarding the surface dechanneling and the dechanneling as a function of depth. Damage was introduced by 2-MeV He^+ incident in a random direction and the resultant increase of the dechanneling rate was studied as a function of damage dose. It is found that the dechanneling is mainly due to defect clusters produced in energetic displacement cascades. A dechanneling cross section of $\sigma_d = 2.3 \times 10^{-14}$ cm^2 is derived under the assumption that all of the dechanneling is due to the clusters visible by transmission electron microscopy (TEM). The dechanneling cross section is about a factor of 5 smaller than the geometrical cross section of the clusters as determined by TEM. Deviations from linearity in the dechanneling-rate–versus–dose curve are noticeable at 5×10^{15} He^+/cm^2. An analysis of the saturation behavior gave a value of $r_0 = 89$ Å for the average radius of a displacement cascade.

I. INTRODUCTION

In recent years the backscattering technique has been used successfully for investigating damage distributions in semiconductors.[1–4] The purpose of the present investigation was to see whether the backscattering method could also be usefully employed in the study of radiation damage in metals.

Contrary to some semiconductors and insulators, the direct backscattering from interstitials is expected to play a minor role in metals. Here the interstitial concentrations will at most be on the order of 1%, even in irradiations at low temperature, while amorphization due to bombardment has been observed in quite a number of covalently bonded systems.[4–7] On the other hand, stable defect structures (e.g., small dislocation loops and voids) are often formed by irradiation in metals as well as nonmetals. The strain fields associated with these defects will distort the channels and cause dechanneling. In fact, dechanneling due to various kinds of lattice defects has been studied in the past, mainly by Quéré and co-workers,[8,9] using transmission experiments.

In the present paper we have used 2-MeV He^+ ions for the dual purpose of introducing damage clusters in thin gold films and as an analyzing beam in the single-alignment backscattering mode. It is well known from transmission electron microscope (TEM) investigations[10–14] that defect clusters $\gtrsim 15$ Å in diameter can be formed in energetic displacement cascades. From the known cluster-formation cross sections and the observed dechanneling rates, we shall be able to derive an average dechanneling cross section σ_d for a cascade cluster. The latter are formed by collapse or rearrangement of vacancies within the depleted zone[15] and their size is, therefore, not directly related to the total volume that has been affected by the displacement processes within a cascade. However, the average cascade volume can be deduced from the dose dependence of the dechanneling rate. Apart from the obvious interest from the point of view of radiation damage, beam damage as observed here is of importance in many channeling experiments and in many solid-state experiments where the channeling-effect technique is used as an analytical tool.

II. EXPERIMENTAL

Single-crystalline gold films of (001) orientation were grown in a ultrahigh-vacuum evaporation system by epitaxy on cleavage surfaces of NaCl single crystals. The gold film thickness was $t = 4820$ Å as determined gravimetrically. The transfer to small disks with 1-mm apertures was accomplished by means of the Noggle technique.[16] Optical flatness and single crystallinity were checked by laser